The Thioredoxin-1 Inhibitor 1-Methylpropyl 2-Imidazolyl Disulfide (PX-12) Decreases Vascular Permeability in Tumor Xenografts Monitored by Dynamic Contrast Enhanced Magnetic Resonance Imaging

Bénédicte F. Jordan,[1,4] Matthew Runquist,[2] Natarajan Raghunand,[1] Robert J. Gillies,[1] Wendy R. Tate,[3] Garth Powis,[3] and Amanda F. Baker[3]

Departments of [1]Biochemistry and [2]Biotechnology, University of Arizona Health Sciences Center; [3]Arizona Cancer Center, University of Arizona, Tucson, Arizona; and [4]Laboratory of Biomedical Magnetic Resonance, Université Catholique de Louvain, B-1200 Brussels, Belgium

ABSTRACT

Purpose: The purpose of this study was to use dynamic contrast enhanced magnetic resonance imaging (DCE-MRI) to measure changes in tumor xenograft permeability produced by the antitumor thioredoxin-1 (Trx-1) inhibitor 1-methylpropyl 2-imidazolyl disulfide (PX-12) and to assess the relationship to Trx-1 and vascular endothelial growth factor (VEGF) levels.

Experimental Design: DCE-MRI was used to monitor the dynamics of gadolinium-diethylenetriaminepentaacetic acid coupled bovine serum albumin as a macromolecular contrast reagent to measure hemodynamic changes in HT-29 human colon xenografts in immunodeficient mice treated with PX-12. Blood vessel permeability was estimated from the slope of the enhancement curves, and tumor vascular volume fraction from the ordinate. Tumor Trx-1 and VEGF was also measured.

Results: PX-12 caused a rapid 63% decrease in the average tumor blood vessel permeability within 2 hours of administration. The decrease lasted 24 hours and had returned to pretreatment values by 48 hours. The changes in vascular permeability were not accompanied by alterations in average tumor vascular volume fraction. There was a decrease in tumor and tumor-derived VEGF in plasma at 24 hours after treatment with PX-12, but not at earlier time points. However, tumor redox active Trx-1 showed a rapid decline within 2 hours following PX-12 administration that was maintained for 24 hours.

Conclusion: The rapid decrease in tumor vascular permeability caused by PX-12 administration coincided with a decrease in tumor redox active Trx-1 and preceded a decrease in VEGF. DCE-MRI responses to PX-12 in patients of Trx-1 inhibition at early time points and decreased VEGF at later times, may be useful to follow tumor response and even therapeutic benefit.

INTRODUCTION

Dynamic contrast enhanced magnetic resonance imaging (DCE-MRI) can be used to characterize the functional vasculature, providing information about microvessel blood flow, blood volume, and vessel permeability (1, 2). Signal intensity changes within a tumor measured by DCE-MRI employing low molecular weight gadolinium (Gd) compounds that distribute rapidly in the extracellular space have been used to measure tumor vascular permeability and angiogenic properties (3–6). Correlations of DCE-MRI parameters to therapeutic and clinical end points such as histopathologic outcome and patient survival have been reported (7–12). DCE-MRI techniques that use large molecular weight agents designed for prolonged intravascular retention (macromolecular contrast media, MMCM, or blood pool agents) have also been developed (13, 14) and will soon be available for clinical use. MMCM with molecular sizes that approximate some serum proteins experience minimal extraction in normal vessels and are well-suited for the measurement of tumor hyperpermeability (15–19).

Most studies using DCE-MRI have focused upon measuring the effects of vascular endothelial growth factor (VEGF, also known as vascular permeability factor), a cytokine produced by many tumors that stimulates the formation of new blood vessels from the existing vasculature (angiogenesis; ref. 20). Angiogenesis is critical for the growth of solid tumors (21) and increased VEGF expression has been shown to lead to increased tumor angiogenesis, tumor progression, and metastasis (22–24). VEGF expression may also be a predictive factor for decreased patient survival (25). It has been suggested that DCE-MRI can be used as an early biomarker to monitor the response to therapy with anti-VEGF agents and other inhibitors of angiogenesis (6, 26, 27). However, several other factors, could contribute to the high vascularity of tumors including bradykinin (28), tumor necrosis factor-α (29), and interleukin-2 (30). Nitric oxide (NO) produced by endothelial NO synthase (NOS) also plays an important role in mediating the angiogenic and vascular permeability effects of VEGF (31).

Thioredoxin-1 (Trx-1) is a ubiquitously expressed small redox protein with a conserved catalytic site that undergoes

reversible NADPH-dependent reduction by selenocysteine-containing flavoprotein Trx-1 reductases (32). Trx-1 has multiple effects in the cell that includes the regulation of the DNA binding and *trans*-activating activity of redox-sensitive transcription factors such as the glucocorticoid receptor (33), NF-κB (34), p53 (35), hypoxia-inducible transcription factor-1 (HIF-1; 36) and, indirectly through redox factor 1 (Ref-1/HAP1), AP-1 (Fos/Jun heterodimer; ref. 37). Trx-1 binds in a redox-dependent manner to enzymes to regulate their activity including apoptosis signal-regulated kinase-1 (ASK-1; ref. 38), protein kinases Cα, δ, ϵ, and ζ (39), and the tumor suppresser phosphatase and tensin homologue deleted on chromosome 10 (PTEN; 40). Trx-1 also provides reducing equivalents to cytoplasmic thioredoxin peroxidases that protect cells against oxidant-induced apoptosis by scavenging H_2O_2 and organic hydroperoxides (41).

Trx-1 expression is increased in several human cancers, including lung, colon, cervix, liver, pancreatic, colorectal, and squamous cell cancer (32, 42–46). Clinically, increased Trx-1 levels have been linked to aggressive tumor growth, inhibition of apoptosis and decreased patient survival (42–46). 1-Methylpropyl 2-imidazolyl disulfide (PX-12) is an inhibitor of Trx-1 that irreversibly thioalkylates a critical cysteine residue (Cys[73]) that lies outside the conserved redox catalytic site of Trx-1 (47). PX-12 is active as a Trx-1 inhibitor at submicromolar concentrations and has been shown to have *in vivo* antitumor activity against human tumor xenografts including HT-29 colon cancer in severe combined immunodeficient mice (47). PX-12 has recently been tested in a phase I trial in patients with advanced malignancies (48) where it has been shown to decrease plasma Trx-1 and VEGF levels in some patients (49).

The formation of VEGF is regulated in part by the HIF-1 through a HIF-1 binding site in the promoter region of the VEGF gene (50). HIF-1 is a heterodimer of an oxygen-degraded HIF-1α subunit and a stable HIF-1β subunit (51). Trx-1 overexpression increases HIF-1α protein levels under both normoxic and hypoxic conditions and increases HIF-1 trans-activating activity and VEGF production by tumors (36). PX-12 has been shown to cause significant decreases in the expression of HIF-1α and VEGF, and microvessel density in xenograft tumors (52). It was, therefore, of interest for us to study changes in tumor hemodynamic properties caused by PX-12 using DCE-MRI with the MMCM, Gd-DTPA coupled to albumin Gd-bovine serum albumin (BSA), and to investigate the relationship of the DCE-MRI changes to Trx-1 and VEGF levels. We report that PX-12 causes a rapid and sustained decrease in tumor vascular permeability that correlates with a decrease in tumor Trx-1 activity, but that tumor VEGF levels did not decrease until several hours later.

MATERIALS AND METHODS

Cell Line and Tumor Implantation. HT-29, a tumorigenic, nonmetastatic colon carcinoma cell line was obtained from the American Tissue Type Collection (Rockville, MD). Cells were passaged twice weekly with a 1:2 split and cultured in DMEM supplemented with 10% fetal bovine serum (HyClone, Ft. Collins, CO). For inoculation, approximately 10^6 cells in 0.1 mL of media were injected s.c. into the right flank of female severe combined immunodeficient mice of ages 5 to 6 weeks (obtained from the Arizona Cancer Center Experimental Mouse Shared Service). Mice developed palpable tumors within a week of inoculation. Tumors were allowed to grow to 100 to 500 mm^3 prior to imaging. All animal protocols were approved by the University of Arizona Institutional Animal Care and Use Committee (IACUC).

Treatment. PX-12 was provided by Prolx Pharmaceuticals (Tucson, AZ). Mice were treated with either vehicle (7% polyethylene glycol 400 in 0.013 N HCl) or with 25 mg/kg PX-12 (2.5 mg/mL in vehicle) i.v. and were studied 2, 12, 24, or 48 hours later. For imaging, mice (three control and three treated for each time point) were anesthetized using 1.0% to 2.0% isoflurane carried in oxygen. Body temperature was maintained at 37°C with a circulating water blanket and was monitored using a rectal fluoroptic thermometer (Luxtron, Santa Clara, CA). The contrast agent Gd-BSA, 0.6 mg/g in 0.15 mL saline, was injected via a tail vein catheter comprising a 30-gauge needle connected to PE-20 polyethylene tubing. The Gd-BSA was synthesized by the Arizona Cancer Center Synthetic Chemistry Core.

DCE-MRI Data Acquisition. All imaging was done on a 4.7 T horizontal bore MR imager (Bruker, Billerica, MA; ref. 53). Mice were positioned into a 24 mm ID Litzcage coil (Doty Scientific, Columbia, SC). Sagittal scout images were obtained to determine the position of the tumors. Contiguous axial 2.0 mm slices covering the entire tumor, as well as one slice through the kidneys, were imaged by the following protocol; a proton-density-weighed (TR = 8 seconds, TE = 5.9 milliseconds, NA = 2, FOV = 4 × 4 cm) and a T_1 weighed spin-echo image (TR = 300 milliseconds, TE = 5.9 milliseconds, NA = 8, FOV = 4 × 4 cm) collected prior to injection of contrast agent. A dynamic series of spin-echo images (TR = 300 milliseconds, TE = 5.9 milliseconds, NA = 4, FOV = 4 × 4 cm, NR = 19) were collected over 45 minutes, with the contrast agent solution being injected during repetitions two to five.

DCE-MRI Data Analysis. Figure 1 gives the basis for DCE-MRI signal enhancement with MMCM. Extravasation of the Gd-BSA was assumed to be described by a permeability-limited two-compartment model with unidirectional transport of contrast agent on the time scale of the study. Signal enhancement in the DCE-MRI data was converted to Gd-BSA concentration using the relaxivity measured *in vitro* at 37°C (1.08 L/g/s) assuming a linear relationship between Gd concentration and relaxation rate enhancement. The Gd-BSA versus time data was fitted to a straight line for each pixel, to obtain a *slope* (related to vascular permeability) and *y*-axis intercept (related to the vascular volume; ref. 53).

The slope of enhancement in the vena cava was calculated and normalized for Gd dose using the slope determined in the tumor for each mouse. The vena cava was identified using a hand-drawn region of interest of approximately 5 to 10 pixels. The vascular volume parameter measured in the tumor was divided by the value obtained in the muscle and multiplied by 5% (the approximate vascular volume fraction of the muscle) to obtain the vascular volume fraction of the tumor. Permeability and vascular volume fraction maps were generated. Data analysis was done using programs written in Interactive Data Language (Research Systems, Boulder, CO).

Fig. 1 DCE-MRI enhancement with MMCM. Individual imaging voxels (*boxes A-E*) containing a blood vessel with arterial (*red*) to venous (*blue*) flow. In areas with vascular imperfections leading to leakiness (*spots*), the MMCM extravasates into the interstitial space. The corresponding enhancement curves are shown below each voxel. The *Y*-intercept is an estimate of the vascular volume and the slope is an estimate of the permeability.
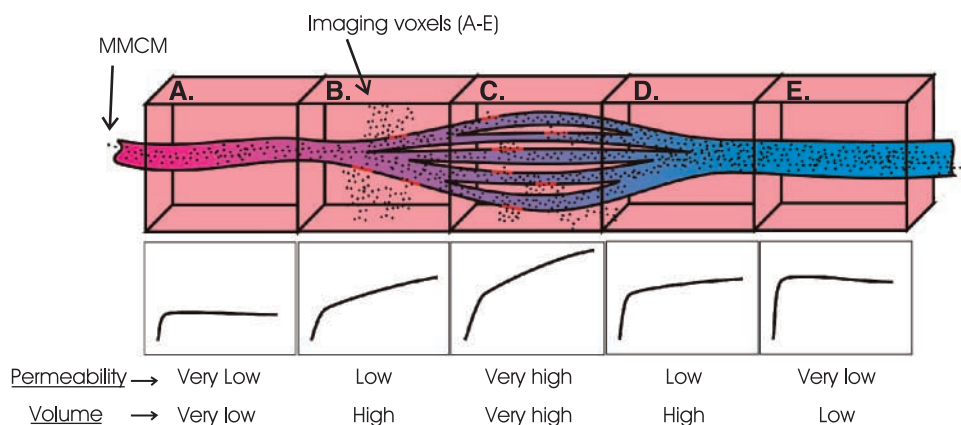
VEGF and Trx-1 Measurements. HT-29 xenograft tumors were grown to approximately 400 mm^3 as described above. Mice were treated with 25 mg/kg PX-12 and sacrificed at various times. Blood was collected into EDTA tubes and tumors removed and immediately snap-frozen and stored in liquid nitrogen. For assay, the tumors were homogenized using a PowerGen 125 homogenizer (Fisher Scientific, Pittsburgh, Pennsylvania) in 10 mmol Tris-HCl buffer (pH 7.4), 100 mmol NaCl. The suspension was centrifuged twice at $8,000 \times g$ at 4°C for 15 minutes and protein in the supernatant measured using Coomassie protein assay reagent (Pierce Biotechnology, Rockford, IL). Tumor total Trx-1 was measured by Western blotting using a mouse anti-human Trx-1 monoclonal antibody (5A3G5) that does not distinguish between free and PX-12-bound Trx-1 (46). Detection was with donkey anti-rabbit IgG peroxidase coupled secondary antibody and the Renaissance chemiluminescence system on Kodak X-Omat Blue XB films (Eastman Kodak, New Haven, CT). Bands were quantified using Eagle Eye software (Stratagene Corp., La Jolla, CA). Actin was used as a loading control. Tumor redox active Trx-1 was measured spectrophotometrically as the rate of oxidation of NADPH at 339 nm by human placental thioredoxin reductase, as previously described (54). Results are expressed as micrograms of Trx-1 per milligram of cellular protein calculated from the rate of reduction of recombinant human Trx-1 in the same assay. Tumor VEGF levels were measured in plasma and tumor lysates using human VEGF and mouse VEGF ELISA kits (R&D Systems, Minneapolis, MN) according to the manufacturer's instructions.

RESULTS

DCE-MRI Response. Parameter maps of vascular permeability and vascular volume fraction were created to visualize tumor hemodynamic parameters. Figure 2*A* is a typical series of permeability maps 2 hours after vehicle or PX-12, 25 mg/kg, administration showing there are areas of high and low permeability within a tumor. Heterogeneities in the distribution of tumor hemodynamic parameters have previously been reported in experimental as well as in human tumors (55, 56). PX-12 treatment caused a rapid decrease within 2 hours in permeability in all areas of the tumor. At the same time, there was no change in muscle or kidney vascular

permeability which was always much lower than in the tumor. PX-12 administration had no effect upon the average tumor vascular volume fraction (Fig. 2*B*).

Histogram analyses of the data loses the spatial information yet retains the distribution of values for quantitative analyses. Figure 3 shows histogram data summed for all animals in each group. Control tumors (*open columns*) were characterized by heterogeneous and broad distributions of permeability values, and this was invariant between time points. In contrast, PX-12-treated tumors showed homogeneous and narrow histograms centered around much lower values. The distribution of permeability values returned to control levels within 48 hours.

When averaged across all tumors there was as a rapid decrease, within 2 hours of PX-12 administration, in tumor blood vessel permeability compared with control or vehicle-treated tumors with a mean decrease ($\pm$SD) of $63.4 \pm 11.3\%$ ($P < 0.01$; Fig. 4*A*). The decrease in tumor blood vessel permeability was still present 12 hours after PX-12 administration with a mean decrease of $59.2 \pm 11.2\%$ ($P < 0.01$), but progressively lessened at the later time points, with a mean decrease of $51.6 \pm 7.2\%$ ($P < 0.05$) at 24 hours and had returned to control values at 48 hours ($103.4 \pm 17.6\%$, not significant). The vascular volume fraction of the tumor was not significantly modified at any time point (Fig. 4*B*).

VEGF and Trx-1. The effect of PX-12 administration upon tumor Trx-1 is shown in Fig. 5. There was no change in total Trx-1 protein in the tumor except a small nonsignificant decrease of 29% at 48 hours following treatment with PX-12 at 25 mg/kg i.v. However, there was a marked and rapid decrease in tumor redox active Trx-1 within 2 hours of PX-12 administration, to $18.2 \pm 6.5\%$ of control values, that was still $60.1 \pm 12.5\%$ of control values at 48 hours ($P < 0.01$ in both cases). There was a decrease in tumor human VEGF by 24 hours after PX-12 administration with below detectable levels (1 pg per microgram of protein), but not at the earlier time points of 2 and 12 hours (Fig. 6). Low levels of mouse VEGF in the tumor, presumably derived from mouse blood, stromal tissue, and endothelial cells, did not show a significant change at any time point. Mouse VEGF in plasma exhibited a decrease to $49.9 \pm 12.5\%$ of pretreatment values at 24 hours ($P < 0.05$) but was not significantly changed at the other time points. Human VEGF could not be detected in mouse plasma.
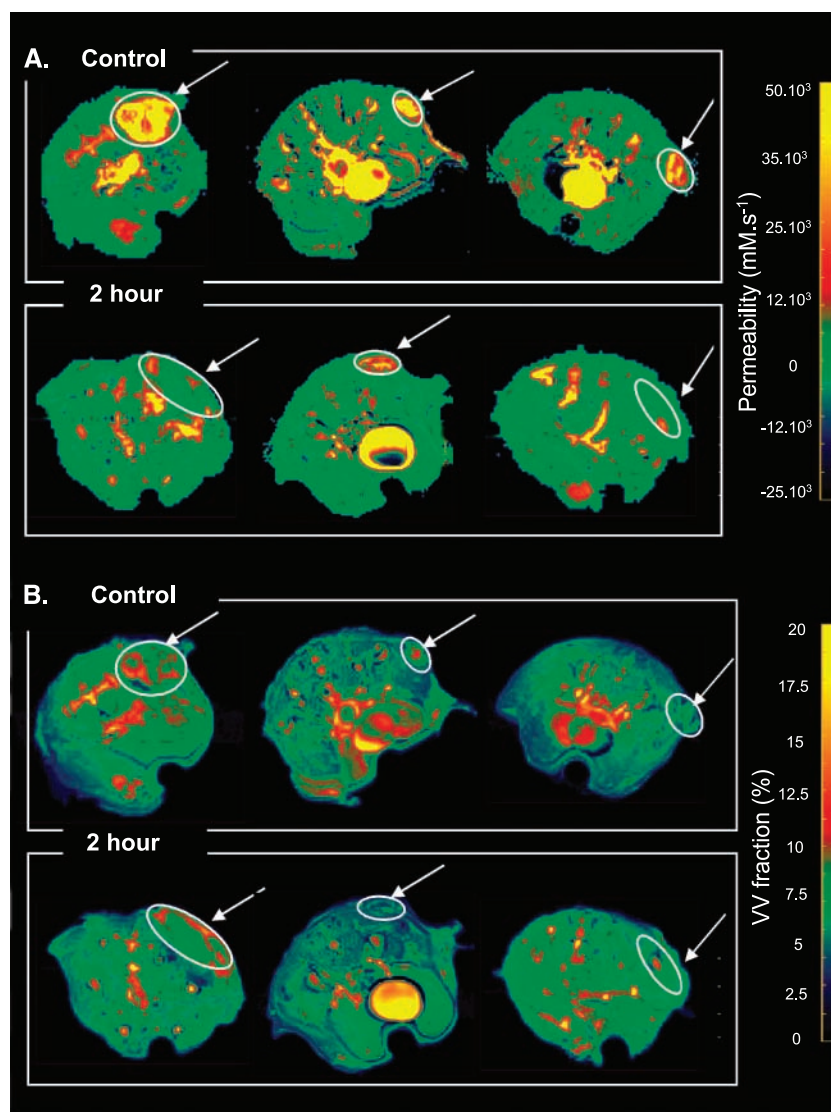
Fig. 2 Vascular permeability and vascular volume fraction maps of tumors treated with PX-12. *A,* vascular permeability maps 2 hours after vehicle (*control*) or treatment with PX-12 (25 mg/kg). Each image is an axial slice of the mouse with the tumor area encircled (*arrow*). There was a substantial reduction in tumor vascular permeability in PX-12-treated tumors compared with vehicle-treated tumors. *B,* vascular volume fraction maps 2 hours after vehicle (*control*) or PX-12 administration. There is no change in the average vascular volume fraction after treatment is seen.

DISCUSSION

PX-12 is an investigational cancer drug that inhibits Trx-1 and Trx-1 redox signaling (47). PX-12 has also been shown to decrease HIF-1α protein levels as well as the expression of HIF-1 downstream target genes such as VEGF, and to decrease microvessel density in different tumor models including HT-29 human colon carcinoma xenografts (52). In a phase I study in patients with advanced malignancies, PX-12 showed inhibition of tumor growth and decreased plasma Trx-1 and VEGF levels in some patients (49).

Macromolecular DCE-MRI can be used to follow changes in tumor vascular permeability and vascular volume fraction induced by antiangiogenic therapies (57). In a clinical study using DCE-MRI to monitor the antivascular effects of anti-VEGF antibody treatment large reductions in tumor vascular permeability were seen within 24 hours of a 3-day treatment that were not accompanied by a change in fractional plasma volume (58). Both intermediate and large molecular contrast agents can be used to monitor tumor response to VEGF antibodies in experimental tumors where significant reductions in tumor vascular permeability as well as in fractional plasma volume were observed (19). In the present study, DCE-MRI with Gd-BSA as the MMCM was used to assess hemodynamic changes in HT-29 tumor xenografts after treatment with PX-12. The results showed a significant decrease in tumor vascular permeability, within 2 hours of PX-12 administration, which persisted for 24 hours with a return to pretreatment values by 48 hours. The vascular volume fraction was not affected by PX-12 at any time point.

The very rapid decrease in tumor vascular permeability following PX-12 administration is unlikely to have been caused by a decrease in VEGF synthesis. Tumor HIF-1α, whose breakdown in posttranslationally regulated, shows a decrease 4 hours following PX-12 administration (52). Although VEGF mRNA and protein have half lives of around 30 minutes (59, 60) and can show relatively rapid changes, we found that tumor VEGF-A levels did not decrease significantly until 24 hours after PX-12 treatment. A caveat is that the ELISA assay recognizes
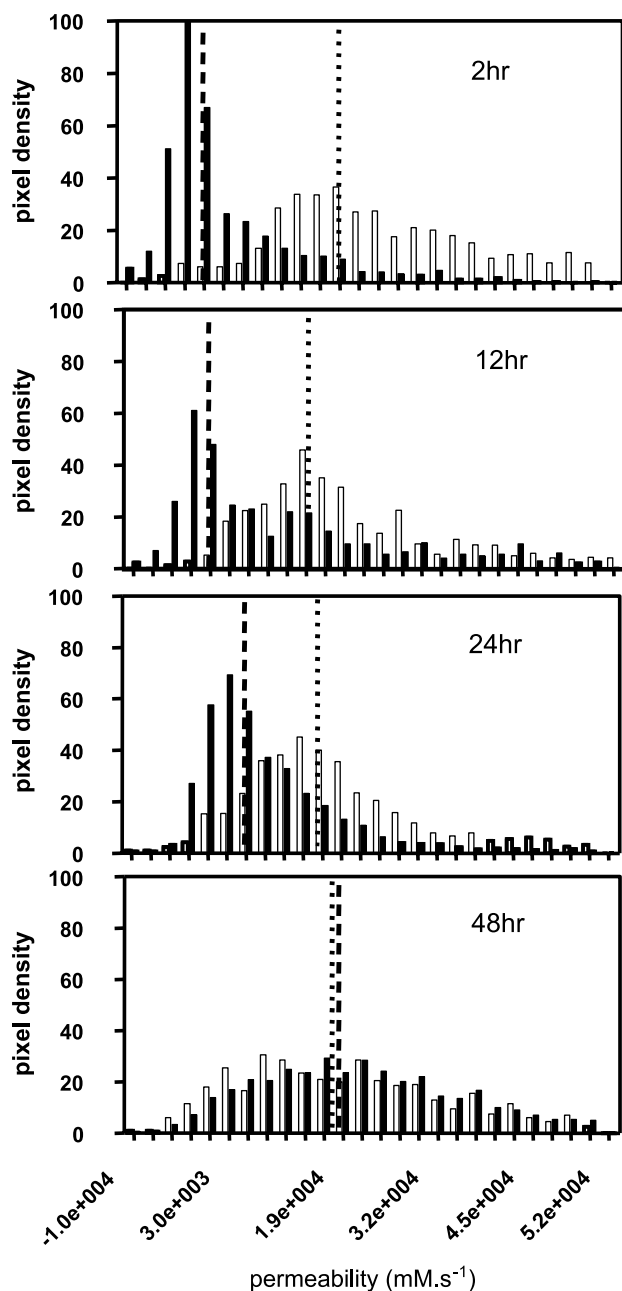
Fig. 3 Summed histograms of the hemodynamic changes caused by PX-12. *Open columns,* vehicle control tumors; *filled bars,* PX-12-treated tumors. Values are the mean of three mice.

VEGF-A 121, 165, and 206 splice isoforms but not 145 and 189 isoforms, and it is possible that other forms of VEGF could be responsible for the hemodynamic changes. There was however, no change in VEGF-A or VEGF-C gene expression 2 hours after PX-12 treatment (not shown). PX-12 could be inhibiting the production of other vascular permeability factors. We have previously reported that PX-12 inhibits the expression of inducible NOS in cultured cells (52). NO formed by inducible NOS increases vascular permeability (61). However, it seems unlikely that a decrease in inducible NOS expression could occur

with the rapid time course seen for the decreased tumor vascular permeability following PX-12 administration. NO synthases contain vicinal cysteine residues that in the presence of NO undergo *S*-nitrosylation and disulfide formation resulting in inhibition of catalytic activity. Trx-1 has been shown to restore the catalytic activity of NO-exposed NO synthase as purified enzyme and in pulmonary artery endothelial cells (62). It is possible therefore, that by inhibiting the redox activity of Trx-1, PX-12 causes decreased NO synthase activity and decreased NO formation. Alternatively, PX-12 might directly inhibit NO synthase by promoting vicinal cysteine disulfide formation.

Although we saw no correlation between the decrease in tumor vascular permeability caused by PX-12 and a decrease in VEGF levels at early time points, we did see a rapid decrease in tumor Trx-1 redox activity by PX-12. Trx-1 which has not previously been reported to affect vascular permeability is a secreted protein (63) and can enhance the growth-stimulating effects of cytokines such as interleukin-2 in cancer cells (64). Interleukin-2 increases the permeability of vascular endothelium
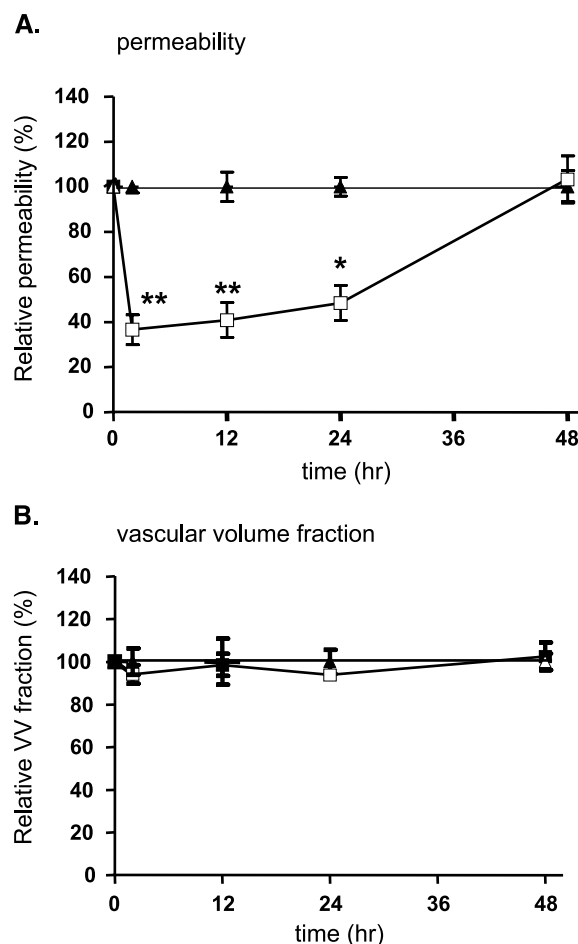

Fig. 4 Time course of tumor hemodynamic changes caused by PX-12. Mice received vehicle alone or PX-12 (25 mg/kg). *A,* vascular permeability estimated from the slope of the enhancement curves; *B,* vascular volume fraction was estimated from the ordinate. (▲) Vehicle control and (□) PX-12-treated tumors in both cases. There were three mice in each group. *Bars,* SD; *, $P < 0.05$; **, $P < 0.01$.
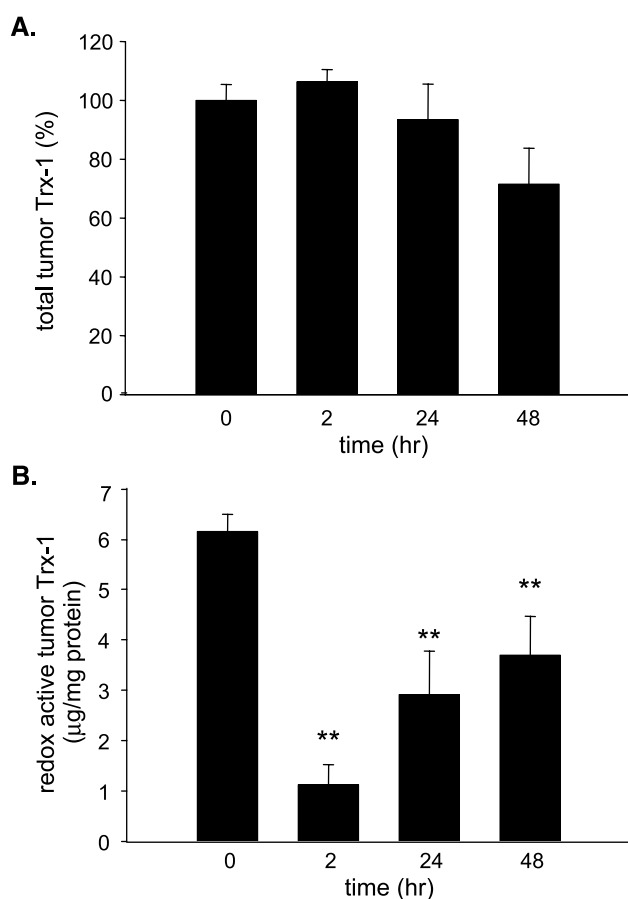
A.

B.

Fig. 5 Effect of PX-12 on tumor Trx-1. Mice were treated with PX-12 (25 mg/kg i.v.) and (*A*) total Trx-1 protein and (*B*) redox active Trx-1 in the tumors measured. Values are the mean of four mice; *bars*, SD. **, $P < 0.01$.

Fig. 6 Effect of PX-12 on VEGF levels in HT-29 tumor xenografts and plasma. Mice were treated with PX-12 (25 mg/kg). (●) Mouse VEGF in plasma (pg/μL); (○) mouse VEGF in the tumor (pg/mg); and (▼) human VEGF in the tumor (pg/mg). *Points,* mean of four mice; *bars,* SD; **, $P < 0.01$.

(65, 66) so that PX-12 might be inhibiting an action of Trx-1 on interleukin 2 that in turn leads to decreased vascular permeability.

Another explanation for the decrease in vascular permeability by PX-12 is that it has a direct effect on the vascular endothelium perhaps inhibiting the VEGF receptor or VEGF receptor signaling. If so, this is likely to be a relatively specific effect because *N*-ethylmaleimide, a nonspecific thiol inhibitor, increases vascular permeability when given to rats (67). Although the acute effects of PX-12 on tumor vascular permeability do not seem to be mediated by an effect on VEGF levels, we cannot rule out the possibility that the longer term effects of PX-12 may be related to a decrease in tumor VEGF formation.

We found that PX-12 produced no reduction in tumor vascular volume fraction. Other investigators have also observed this pattern of response following administration of antiangiogenic treatments, such as PTK787/KZ222854 an inhibitor of the VEGF-receptor 1 (VEGF-R1, FLT-1) and VEGF receptor-2 (KDR) tyrosine kinases in an experimental breast cancer model (68). However, the lack of change in fractional plasma volume is not a function of the tumor model, because SU6668 a inhibitor of VEGF receptor-2, fibroblast growth factor receptor-1 and
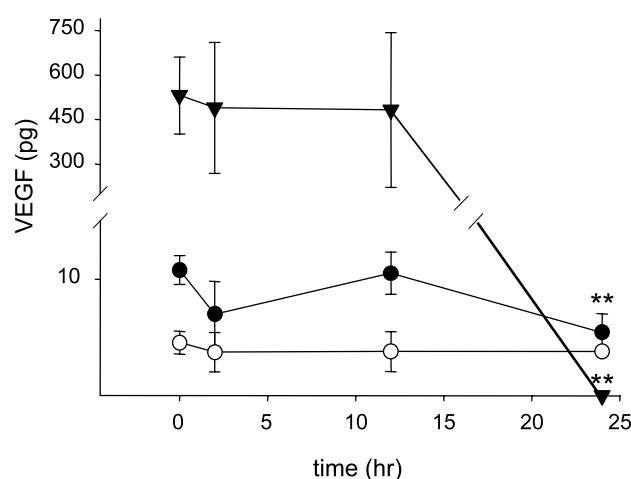
platelet-derived growth factor receptor β tyrosine kinases, in this same system caused a decrease in DCE-MRI measured vessel permeability as well as in fractional plasma volume by 24 hours posttreatment (69).

Although several DCE-MRI studies have shown a decrease in tumor vascular permeability by antiangiogenic therapies, they have generally measured changes 24 hours or more after drug administration (26, 27). However, there are studies that report rapid decreases in tumor vascular permeability within 3 hours of administration of the tumor necrosis factor-α activator 5,6-dimethylxanthenone-4-acetic acid (70), within 4 to 6 hours for the vascular targeting agent combrestatin phosphate A-4 (71), and 6 hours for ZD6126, also a vascular targeting agent (72). However, none of these agents requires altered protein synthesis for their activity. The relevance of DCE-MRI changes, whether short or long-term, to clinical response has yet to be established. Nonetheless, DCE-MRI time course studies in experimental models may be helpful in the design of clinical trials and imaging end points. From this study, we can speculate that DCE-MRI studies of tumor hemodynamics in PX-12-treated patients will be of particular interest in the clinic.

In summary, we have shown using DCE-MRI and the MMCR Gd-BSA in mice that the Trx-1 inhibitor PX-12 causes a rapid decrease in HT-29 colon tumor xenograft blood vessel permeability within 2 hours of administration. The decrease lasted 24 hours and had returned to pretreatment values by 48 hours. The changes in vascular permeability were not accompanied by alterations in average tumor vascular volume fraction. There was no change in tumor or plasma VEGF at the early time points after PX-12 treatment but there was a rapid decrease in tumor Trx-1 that was maintained for 24 hours. Thus, the decreased tumor permeability at earlier time points may be due to a decrease in Trx-1 although a contribution of decreased VEGF at later time points cannot be ruled out.

REFERENCES

1. Evelhoch JL, Gillies RJ, Karczmar GS, et al. Applications of magnetic resonance in model systems: cancer therapeutics. Neoplasia 2000;2:152–65.

2. Gillies RJ, Bhujwalla ZM, Evelhoch J, et al. Applications of magnetic resonance in model systems: tumor biology and physiology. Neoplasia 2000;2:139–51.

3. Brasch RC, Li KC, Husb JE, et al. *In vivo* monitoring of tumor angiogenesis with MR imaging. Acad Radiol 2000;7:812–23.

4. Neeman M, Provenzale JM, Dewhirst MW. Magnetic resonance imaging applications in the evaluation of tumor angiogenesis. Semin Radiat Oncol 2001;11:70–82.

5. Su MY, Cheung YC, Fruehauf JP, et al. Correlation of dynamic contrast enhancement MRI parameters with microvessel density and VEGF for assessment of angiogenesis in breast cancer. J Magn Reson Imaging 2003;18:467–77.

6. Checkley D, Tessier JJ, Kendrew J, Waterton JC, Wedge SR. Use of dynamic contrast-enhanced MRI to evaluate acute treatment with ZD6474, a VEGF signaling inhibitor, in PC-3 prostate tumours. Br J Cancer 2003;17;89:1889–95.

7. Buadu LD, Murakami J, Murayama S, et al. Breast lesions: correlation of contrast medium enhancement patterns on MR images with histopathologic findings and tumor angiogenesis. Radiology 1996;200:639–49.

8. Hawighorst H, Weikel W, Knapstein PG, et al. Angiogenic activity of cervical carcinoma: assessment by functional magnetic resonance imaging-based parameters and a histomorphological approach in correlation with disease outcome. Clin Cancer Res 1998;4:2305–12.

9. Mayr NA, Hawighorst H, Yuh WT, Essig M, Magnotta VA, Knopp MV. MR microcirculation assessment in cervical cancer: correlations with histomorphological tumor markers and clinical outcome. J Magn Reson Imaging 1999;10:267–76.

10. Gossmann A, Helbich TH, Kuriyama N, et al. Dynamic contrast-enhanced magnetic resonance imaging as a surrogate marker of tumor response to anti-angiogenic therapy in a xenograft model of glioblastoma multiforme. J Magn Reson Imaging 2002;15:233–40.

11. Morgan B, Thomas AL, Drevs J, et al. Dynamic contrast-enhanced magnetic resonance imaging as a biomarker for the pharmacological response of PTK787/ZK 222584, an inhibitor of the vascular endothelial growth factor receptor tyrosine kinases, in patients with advanced colorectal cancer and liver metastases: results from two phase I studies. J Clin Oncol 2003;21:3955–64.

12. Kiessling F, Farhan N, Lichy MP, et al. Dynamic contrast-enhanced magnetic resonance imaging rapidly indicates vessel regression in human squamous cell carcinomas grown in nude mice caused by VEGF receptor 2 blockade with DC101. Neoplasia 2004;6:213–23.

13. Ogan MD. Albumin labeled with Gd-DTPA: an intravascular contrast-enhancing agent for magnetic resonance blood pool imaging: preparation and characterization. Invest Radiol 1988;23:961.

14. Brasch R, Pham C, Shames D, et al. Assessing tumor angiogenesis using macromolecular MR imaging contrast media. J Magn Reson Imaging 1997;7:68–74.

15. Demsar F, Roberts TP, Schwickert HC, et al. A MRI spatial mapping technique for microvascular permeability and tissue blood volume based on macromolecular contrast agent distribution. Magn Reson Med 1997;37:236–42.

16. Su MY, Muhler A, Lao X, Nalcioglu O. Tumor characterization with dynamic contrast-enhanced MRI using MR contrast agents of various molecular weights. Magn Reson Med 1998;39:259–69.

17. Daldrup H, Shames DM, Wendland M, et al. Correlation of dynamic contrast-enhanced MR imaging with histologic tumor grade: comparison of macromolecular and small-molecular contrast media. AJR Am J Roentgenol 1998;171:941–9.

18. Gossmann A, Okuhata Y, Shames DM, et al. Prostate cancer tumor grade differentiation with dynamic contrast-enhanced MR imaging in the rat: comparison of macromolecular and small-molecular contrast media-preliminary experience. Radiology 1999;213:265–72.

19. Roberts TP, Turetschek K, Preda A, et al. Tumor microvascular changes to anti-angiogenic treatment assessed by MR contrast media of different molecular weights. Acad Radiol 2002;9 Suppl 2:S511–3.

20. Ferrara N, Gerber H-P, LeCouter J. The biology of VEGF and its receptors. Nat Med 2003;9:669–84.

21. Dachs GU, Tozer GM. Hypoxia modulated gene expression: angiogenesis, metastasis and therapeutic exploitation. Eur J Cancer 2000;36:1649–60.

22. Yonemura Y, Endo Y, Fujita H, et al. Role of vascular endothelial growth factor C expression in the development of lymph node metastasis in gastric cancer. Clin Cancer Res 1999;5:1823–9.

23. Gisselbrecht C, Likiec F, Marty M, et al. Cancer Chemother Pharmacol 1980;5:20.

24. Wong MP, Cheung N, Yuen ST, Leung SY, Chung LP. Vascular endothelial growth factor is upregulated in early premalignant stage of colorectal tumour progression. Int J Cancer 1999;81:845–50.

25. Wang G, Dong Z, Xu G, et al. The effect of antibody against vascular endothelial growth factor on tumor growth and metastasis. J Cancer Res Clin Oncol 1998;124:615–20.

26. Dowlati A, Robertson K, Cooney M, et al. A phase I pharmacokinetic and translational study of the novel vascular targeting agent combretastatin A-4 phosphate on a single dose intravenous schedule in patients with advanced cancer. Cancer Res 2002;62:3408–16.

27. Morgan B, Thomas AL, Drevs J, et al. Dynamic contrast-enhanced magnetic resonance imaging as a biomarker for the pharmacological response of PTK787/ZK 222584, an inhibitor of the vascular endothelial growth factor receptor tyrosine kinases, in patients with advanced colorectal cancer and liver metastases: results from two phase I studies. J Clin Oncol 2003;21:3955–64.

28. Dewhirst MW, Vinuya RZ, Ong ET, et al. Effects of bradykinin on the hemodynamics of tumor and granulating normal tissue microvasculature. Radiat Res 1992;130:345–54.

29. Ettinghausen SE, Puri RK, Rosenberg SA. Increased vascular permeability in organs mediated by the systemic administration of lymphokine activated killer cell and recombinant interleukin-1 in mice. J Natl Cancer Inst 1988;80:177–88.

30. Yuan F, Salehi HA, Boucher Y, Vasthare HS, Tuma RF, Jain RK. Vascular permeability and microcirculation of gliomas and mammary carcinomas transplanted in rat and mouse cranial windows. Cancer Res 1994;54:4565–8.

31. Fukumura D, Gohongi T, Kadambi A, et al. Predominant role of endothelial nitric oxide synthase in vascular endothelial growth factor-induced angiogenesis and vascular permeability. Proc Natl Acad Sci U S A 2001;98:2604–9.

32. Powis G, Montfort WR. Properties and biological activities of thioredoxins. Annu Rev Pharmacol Toxicol 2001;41:261–95.

33. Grippo JF, Tienrungroj W, Dahmer MK, Housley PR, Pratt WB. Evidence that the endogenous heat-stable glucocorticoid receptor-activating factor is thioredoxin. J Biol Chem 1993;258:13658–64.

34. Qin J, Clore GM, Kennedy WP, Hutch JR, Gronenborn AM. Solution structure of human thioredoxin in a mixed disulfide intermediate complex with its target peptide from the transcription factor NF-κB. Structure 1994;3:289–97.

35. Ueno M, Masutani H, Jun Arai R, et al. Thioredoxin-dependent redox regulation of p53-mediated p21 activation. J Biol Chem 2001;274:35809–15.

36. Welsh SJ, Bellamy WT, Briehl MM, Powis G. The redox protein thioredoxin-1 (Trx-1) increases hypoxia-inducible factor 1α protein expression: Trx-1 overexpression results in increased vascular endothelial growth factor production and enhanced tumor angiogenesis. Cancer Res 2002;62:5089–95.

37. Abate C, Patel L, Rauscher FJ, Curran T. Redox regulation of fos and jun DNA-binding activity *in vitro*. Science 1990;249:1157–61.

38. Saitoh M, Nishitoh H, Fujii M, et al. Mammalian thioredoxin is a direct inhibitor of apoptosis signal-regulating kinase (ASK) 1. EMBO J 1998;17:2596–606.

39. Watson JA, Rumsby MG, Wolowacz RG. Phage display identifies thioredoxin and superoxide dismutase as novel protein kinase C-interacting proteins: thioredoxin inhibits protein kinase C-mediated phosphorylation of histone. Biochem J 1999;343:301–5.

40. Meuillet E, Mahadevan D, Berggren M, Coon A, Powis G. Thioredoxin-1 binds to the C2 domain of PTEN inhibiting PTEN's lipid phosphatase activity and membrane binding: providing a mechanism for the functional loss of PTEN's tumor suppressor activity. Arch Biochem Biophys 2004;429:123–33.

41. Chae HZ, Kim HJ, Kang SW, Rhee SG. Characterization of three isoforms of mammalian peroxiredoxin that reduce peroxides in the presence of thioredoxin. Diabetes Res Clin Pract 1999;45:101–12.

42. Nakamura H, Bai J, Nishinaka Y, et al. Expression of thioredoxin and glutaredoxin, redox-regulating proteins, in pancreatic cancer. Cancer Detect Prev 2000;24:53–60.

43. Nakamura H, Masutani H, Tagaya Y, et al. Expression and growth-promoting effect of adult T-cell leukemia-derived factor. A human thioredoxin homologue in hepatocellular carcinoma. Cancer 1992;69: 2091–7.

44. Kakolyris S, Giatromanolakim A, Koukourakis M, et al. Thioredoxin expression is associated with lymph node status and prognosis in early operable non small cell lung cancer (NSCLC). Clin Cancer Res 2001;7:3087–91.

45. Grogan TM, Fenoglio-Prieser C, Zeheb R, et al. Thioredoxin, a putative oncogene product, is overexpressed in gastric carcinoma and associated with increased proliferation and increased cell survival. Hum Pathol 2000;31:475–81.

46. Raffel J, Bhattacharyya AB, Gallegos A, et al. Increased expression of thioredoxin-1 in human colorectal cancer is associated with decreased patient survival. J Lab Clin Med 2002;142:46–51.

47. Kirkpatrick DL, Kuperus M, Dowdeswell M, et al. Mechanisms of inhibition of the thioredoxin growth factor system by antitumor 2-imidazolyl disulfides. Biochem Pharmacol 1998;55:987–94.

48. Kirkpatrick L, Dragovich T, Ramahathan R, et al. Results from phase I study of PX-12, a thioredoxin inhibitor in patients with advanced solid malignancies. Proc Am Assoc Clin Oncol 2004;22:217.

49. Baker A, Dragovich T, Tate WR, Kirkpatrick DL, Powis G. Pharmacodynamic proteomic studies of the thioredoxin-1 inhibitor PX-12 in mice and patients. Proc Am Assoc Clin Oncol 2004;22: 3662.

50. Mukhopadhyay D, Datta K. Multiple regulatory pathways of vascular permeability factor/vascular endothelial growth factor (VPF/VEGF) expression in tumors. Semin Cancer Biol 2004;14:123–30.

51. Semenza GL. Targeting HIF-1 for cancer therapy. Nat Rev Cancer 2003;3:721–32.

52. Welsh SJ, Williams RR, Birmingham A, Newman DJ, Kirkpatrick DL, Powis G. The thioredoxin redox inhibitors 1-methylpropyl 2-imidazolyl disulfide and pleurotin inhibit hypoxia-induced factor 1α and vascular endothelial growth factor formation. Mol Cancer Ther 2003;2:235–43.

53. Bhujwalla ZM, Artemov D, Natarajan K, Ackerstaff E, Solaiyappan M. Vascular differences detected by MRI for metastatic versus nonmetastatic breast and prostate cancer xenografts. Neoplasia 2001;3: 143–53.

54. Luthman M, Holmgren A. Rat liver thioredoxin and thioredoxin reductase: purification and characterization. Biochemistry 1982;21: 6628–33.

55. Bhujwalla ZM, Artemov D, Natarajan K, Solaiyappan M, Kollars P, Kristjansen PE. Reduction of vascular and permeable regions in solid tumors detected by macromolecular contrast magnetic resonance imaging after treatment with antiangiogenic agent TNP-470. Clin Cancer Res 2003;9:355–62.

56. Roberts HC, Roberts TP, Brasch RC, Dillon WP. Quantitative measurement of microvascular permeability in human brain tumors achieved using dynamic contrast-enhanced MR imaging: correlation with histologic grade. AJNR Am J Neuroradiol 2000;21:891–9.

57. Padhani AR. Dynamic contrast-enhanced MRI in clinical oncology: current status and future directions. J Magn Reson Imaging 2002;16:407–22.

58. Jayson GC, Zweit J, Jackson A, et al. Molecular imaging and biological evaluation of HuMV833 anti-VEGF antibody: implications for trial design of antiangiogenic antibodies. J Natl Cancer Inst 2002;94:1484–93.

59. Eppler SM, Combs DL, Henry TD, et al. A target mediated model to describe pharmacokinetic and hemodynamic effects of recombinant human vascular endothelial growth factor in humans. Clin Pharmacol Ther 2002;72:20–32.

60. Liu LX, Luo LH, Date T. Stabilization of vascular endothelial growth factor mRNA by hypoxia-inducible factor 1. Biochem Biophys Res Commun 2002:29:908–14.

61. Akaike WJ, Hayashida T, Okamoto T, Okuyama A, Maeda H. Enhanced vascular permeability in solid tumor involving peroxynitrite and matrix metalloproteinases. Jpn J Cancer Res 2001;92:439–51.

62. Patel JM, Zhang J, Block ER. Nitric oxide-induced inhibition of lung endothelial cell nitric oxide synthase via interaction with allosteric thiols: role of thioredoxin in regulation of catalytic activity. Am J Respir Cell Mol Biol 1996;15:410–9.

63. Rubartelli A, Bajetto A, Allavena G, Wollman E, Sitia R. Secretion of thioredoxin by normal and neoplastic cells through a leaderless secretory pathway. J Biol Chem 1992;267:24161–4.

64. Gasdaska JR, Berggren M, Powis G. Cell growth stimulation by the redox protein thioredoxin occurs by a novel helper mechanism. Cell Growth Differ 1995;6:1643–50.

65. Ballmer-Weber B, Dummer R, Kung E, Burg G, Ballmer P. Interleukin 2-induced increase of vascular permeability without decrease of the intravascular albumin pool. Br J Cancer 1995;71:78–82.

66. Downie G, Ryan U, Hayes B, Friedman M. Interleukin-2 directly increases albumin permeability of bovine and human vascular endothelium *in vitro*. Am J Respir Cell Mol Biol 1992;7:58–65.

67. Takeuchi K, Okada M, Niida H, Okabe S. Dual effects of *N*-ethylmaleimide on ethanol-induced gastric lesions in rats. Dig Dis Sci 1991;36:870–9.

68. Turetschek K, Preda A, Floyd E, et al. MRI monitoring of tumor response to a novel VEGF tyrosine kinase inhibitor in an experimental breast cancer model. Acad Radiol 2002;2:S519–20.

69. Marzola P, Degrassi A, Calderan L, et al. *In vivo* assessment of antiangiogenic activity of SU6668 in an experimental colon carcinoma model. Clin Cancer Res 2004;10:739–50.

70. Beauregard DA, Pedley RB, Hill SA, Brindle KM. Differential sensitivity of two adenocarcinoma xenografts to the anti-vascular drugs combretastatin A4 phosphate and 5,6-dimethylxanthenone-4-acetic acid, assessed using MRI and MRS. NMR Biomed 2002;15:99–105.

71. Daldrup-Link H, Okuhata Y, Wolfe A, et al. Decrease in tumor apparent permeability-surface area product to a MRI macromolecular contrast medium following angiogenesis inhibition with correlations to cytotoxic drug accumulation. Microcirculation 2004;11:387–96.

72. DelProposto Z, LoRusso P, Latif Z, et al. MRI Evaluation of the effects of the vascular-targeting agent ZD6126 on tumor vasculature. Proc Am Soc Clin Oncol 2002;21:440.